HHS Public Access

Author manuscript

Nat Microbiol. Author manuscript; available in PMC 2016 August 08.

Published in final edited form as:

Nat Microbiol. 2016 ; 1: . doi:10.1038/nmicrobiol.2015.2.

Crystal structure of *Clostridium difficile* toxin A

Nicole M. Chumbler[1,†], **Stacey A. Rutherford**[2,†], **Zhifen Zhang**[3], **Melissa A. Farrow**[2], **John P. Lisher**[4,5], **Erik Farquhar**[6], **David P. Giedroc**[5], **Benjamin W. Spiller**[1,2,7], **Roman A. Melnyk**[3], and **D. Borden Lacy**[1,2,8,9,*]

[1]Chemical and Physical Biology Program, Vanderbilt University School of Medicine, Nashville, Tennessee 37232, USA

[2]Department of Pathology, Microbiology and Immunology, Vanderbilt University School of Medicine, Nashville, Tennessee 37232, USA

[3]Department of Biochemistry, University of Toronto and the Molecular Structure & Function Research Institute at The Hospital for Sick Children, Toronto, Ontario M5S 1A8, Canada

[4]Interdisciplinary Graduate Program in Biochemistry, Indiana University, Bloomington, Indiana 47405, USA

[5]Department of Chemistry, Indiana University, Bloomington, Indiana 47405, USA

[6]Case Western Reserve University Center for Synchrotron Biosciences, National Synchrotron Light Source, Building 725, Brookhaven National Laboratory, New York 11973, USA

[7]Department of Pharmacology, Vanderbilt University School of Medicine, Nashville, Tennessee 37212, USA

[8]Department of Biochemistry, Vanderbilt University School of Medicine, Nashville, Tennessee 37205, USA

[9]The Veterans Affairs Tennessee Valley Healthcare System, Nashville, Tennessee 37212, USA

Abstract

Clostridium difficile infection is the leading cause of hospital-acquired diarrhoea and pseudomembranous colitis. Disease is mediated by the actions of two toxins, TcdA and TcdB,

*Correspondence and requests for materials should be addressed to D.B.L. borden.lacy@vanderbilt.edu.
†These authors contributed equally to this work.

Author contributions

S.A.R. crystallized $TcdA_{1832}$. S.A.R., B.W.S. and D.B.L. determined the $TcdA_{1832}$ structure. S.A.R., N.M.C. and M.A.F. generated expression clones and purified proteins. N.M.C. and M.A.F. conducted autoprocessing, Rac1 glucosylation and cell binding assays. Z.Z. conducted viability and Rb^+ release assays. N.M.C. prepared samples for ICP-MS assays and J.P.L. performed the assays. E.F. performed XAS measurements. All authors were involved in data analysis and assisted in editing the manuscript. D.B.L. wrote the paper.

Additional information

Supplementary information is available online.

Competing interests

The authors declare no competing financial interests.

Accession numbers. The coordinates for $TcdA_{1832}$ have been deposited in the Protein Data Bank (PDB) database under accession number 4R04.

which cause the diarrhoea, as well as inflammation and necrosis within the colon[1,2]. The toxins are large (308 and 270 kDa, respectively), homologous (47% amino acid identity) glucosyltransferases that target small GTPases within the host[3,4]. The multidomain toxins enter cells by receptor-mediated endocytosis and, upon exposure to the low pH of the endosome, insert into and deliver two enzymatic domains across the membrane. Eukaryotic inositol-hexakisphosphate (InsP6) binds an autoprocessing domain to activate a proteolysis event that releases the N-terminal glucosyltransferase domain into the cytosol. Here, we report the crystal structure of a 1,832-amino-acid fragment of TcdA ($TcdA_{1832}$), which reveals a requirement for zinc in the mechanism of toxin autoprocessing and an extended delivery domain that serves as a scaffold for the hydrophobic α-helices involved in pH-dependent pore formation. A surface loop of the delivery domain whose sequence is strictly conserved among all large clostridial toxins is shown to be functionally important, and is highlighted for future efforts in the development of vaccines and novel therapeutics.

Clostridium difficile is the leading cause of health-care-associated infection in the USA, with clinical outcomes that range from mild diarrhoea to pseudomembranous colitis, toxic megacolon and death[5]. Patients typically respond to treatment with antibiotics such as vancomycin or metronidazole, but recurrence occurs in 25–30% of patients[6] and, in 2011, the infection was linked to 29,000 US deaths[5]. Because CDI is a toxin-mediated disease, a structural and mechanistic understanding of toxin function is a significant priority for the development of novel anti-toxin therapeutics.

TcdA and TcdB are large (308 and 270 kDa, respectively), homologous (47% amino acid identity) proteins with four functional domains that contribute to a multi-step mechanism of entry[4] (Fig. 1a). The C-terminal combined repetitive oligopeptides (CROPS) domain contributes to a cell-surface binding event[7–9], which is followed by receptor-mediated endocytosis[10,11]. The low pH of the endosome promotes the membrane insertion of the central delivery domain, allowing for pore formation[11–13]. The N-terminal glucosyltransferase domain (GTD) is translocated across the membrane and released into the host cell cytosol where it can inactivate small GTPases such as RhoA, Rac1 and Cdc42[14,15]. Release of the GTD from the rest of the toxin is triggered when eukaryotic inositol-hexakisphosphate (InsP6) binds the autoprocessing domain (APD) and activates an intramolecular cleavage reaction[16,17].

Although efforts to obtain well-diffracting crystals of either the TcdA or TcdB holotoxins have been unsuccessful, low-resolution structures of TcdA and TcdB have been determined by electron microscopy (EM) and small-angle X-ray scattering, respectively[18,19]. EM analysis of TcdA and TcdB revealed that the elongated solenoid structure of the CROPS[8,20,21] can adopt multiple conformational states relative to the rest of the protein[18], so we generated a TcdA construct with the CROPS deleted ($TcdA_{1832}$) for crystallization. The structure was determined and refined to 3.25 Å resolution (Supplementary Table 1 and Supplementary Fig. 1), and reveals significant interactions between the GTD and APD and an extended and topologically complex delivery domain (Fig. 1b and Supplementary Video 1). The last residue visible in the $TcdA_{1832}$ structure is S1802. Clear placement of the $TcdA_{4–1802}$ structure into the holotoxin EM structure[18] (Fig. 1d) indicates that the CROPS

extends from the base of the APD and could impact InsP6 binding. This is consistent with reports that the CROPS interacts with N-terminal sequences of TcdA to repress autoprocessing activity[22,23] and our observation that a shorter construct ($TcdA_{1795}$) undergoes autoprocessing more efficiently than TcdA and $TcdA_{1832}$ (Supplementary Fig. 2).

The GTD (residues 1–542) is responsible for transferring a glucose from UDP-glucose to the switch I region of Rho-family GTPases and is similar to the structures of the isolated GTDs from TcdA, TcdB and other large glucosylating toxins (Supplementary Table 2). In the context of $TcdA_{1832}$, the GTD is oriented such that the GTPase binding site (proposed based on mutational studies in the TcdB GTD)[24] is occluded by the presence of the APD (Fig. 1c). This explains data indicating that glucosyltransferase efficiency is enhanced after the GTD is released by autoprocessing[25]. The C-terminus of the GTD emerges in proximity to the APD (residues 543–802), with residues 538–557 forming an extended loop that spans the APD active site (Fig. 2a).

Autoprocessing in TcdA and TcdB has been ascribed to an InsP6-dependent cysteine protease activity that results in cleavage after L542 (L543 for TcdB) and release of the GTD[16,17,26,27]. Structures of the isolated TcdA and TcdB APDs have shown that InsP6 binds a positively charged pocket, distal from the active site[28–30]. Structures in the absence of InsP6 have heretofore been unavailable, but mutational studies have revealed an allosteric switch where InsP6 binding is functionally coupled to the active site through a central 'β-flap' structure (Fig. 2b)[28,30].

The N-terminal portion (547–741) of the $TcdA_{1832}$ APD (crystallized in the absence of InsP6) aligns to the InsP6-bound APD with an alpha-carbon root-mean squared deviation (r.m.s.d.) of 0.67 Å, but the C-terminal portion of the domain is significantly different. The β-flap (residues 746–765) separating the InsP6 binding site and the catalytic dyad (C700 and H655) has rotated ~90° and the sequence that follows (766–802) is significantly repositioned (Fig. 2a,b and Supplementary Video 2). One effect of this conformational change is an increase in positively charged residues at the InsP6 binding site. The pocket transitions from four lysine residues in the $TcdA_{1832}$ structure (K602, K649, K754 and K777) to include seven lysines and one arginine in the InsP6 bound structure (Fig. 2a,b), and thus provides a mechanistic framework for understanding how an electropositive InsP6 binding site can exist in the absence of InsP6. The largest change is evident in Lys766, as its NZ atom moves 21 Å as a result of rearrangements in the β-flap. The change also results in a 19 Å movement of H759 out of the active site (comparison of Cβ atoms). Mutation of H759 (or H757 from TcdB) results in a protein whose autoprocessing profile no longer varies with InsP6 concentration (Fig. 2c), suggesting that this residue is a key regulator of InsP6-induced allostery in TcdA and TcdB.

Analysis of anomalous signals in our diffraction data revealed a zinc atom, bound at H759 and the catalytic dyad of the APD (Fig. 2a and Supplementary Fig. 3a). TcdA binds zinc in solution, as indicated by both X-ray absorption spectroscopy (XAS) and inductively coupled plasma-mass spectrometry (ICP-MS) experiments (Supplementary Fig. 3b and Supplementary Table 3). A zinc atom is present at this site in both TcdA and TcdB, as indicated by ICP-MS analysis of TcdA, TcdB and catalytic dyad mutants (C700A and

H655A or C698A and H653A in TcdA and TcdB, respectively) (Supplementary Table 3). One interpretation for the observation of zinc bound at this site is that zinc acts as an inhibitor of autoprocessing. InsP6 binding could displace His759 (or TcdB His757), causing the release of zinc and the availability of cysteine as a nucleophile. However, the addition of InsP6 to TcdA or TcdB did not displace zinc from the active site (Supplementary Table 3). Furthermore, the removal of the zinc through chelation with *N,N,N′,N′*-tetrakis(2-pyridylmethyl)ethylenediamine (TPEN) resulted in a loss of autoprocessing activity that could then be restored through the addition of zinc (Fig. 2d,f). Even the TcdA H759A and TcdB H757A mutants that retain zinc binding (Supplementary Table 3) were rendered inactive for autoprocessing through treatment with TPEN (Fig. 2e). These experiments indicate that zinc is required for the autoprocessing activity of TcdA and TcdB.

A three-helix bundle (767–841) is located at the GTD–APD interface and serves as a transition into the delivery domain (Fig. 3a). The three-helix bundle is followed by a small globular sub-domain (850–1025) and then an elongated ‘hydrophobic helical stretch’ containing four α-helices (1026–1135) that extend to the other end of the molecule. The delivery domain then adopts a series of β-sheet structures as it returns to the base of the APD (Supplementary Fig. 4). A search for structural homologues using DALI indicates that the delivery domain structure is unique.

The hydrophobic sequences in TcdA (958–1130) and TcdB (956–1128) have been predicted to insert into the endosomal membrane with acidic pH to facilitate the translocation of the GTD into the cytosol[31]. Residues within this stretch have been shown experimentally to be important for TcdB pore formation, and the corresponding residues in TcdA are highlighted in Fig. 3a[32,33]. Recognizing that hydrophobic helical elements resemble motifs present in the pore-forming domain of diphtheria toxin (DT)[34,35], Zhang *et al.* proposed a ‘double-dagger’ model where TcdB inserts two pairs of helical hairpins into the membrane to form a pore[32]. The pore-forming domain of DT is a globular 10-helix bundle, with the most hydrophobic sequences shielded within the core of the soluble toxin structure, while the helical hydrophobic sequences of TcdA are stretched across the surface of an elongated scaffold of β-sheets. We propose that this large delivery domain scaffold provides an alternative structural solution to maintaining hydrophobic segments that are destined for the membrane in a soluble, but readily accessible conformation.

In addition to the homology with TcdB, TcdA shares homology with large glucosylating toxins from *C. sordellii* (TcsH and TcsL), *C. novyi* (Tcnα) and *C. perfringens* (TpeL). Sequences from these six large clostridial toxins (LCTs) were aligned and the sequence conservation was mapped onto the $TcdA_{1832}$ structure (Fig. 3b). The largest area of strict conservation that mapped to the surface of the structure was located in a portion of the ‘hydrophobic helical stretch’, a 1096–1115 loop that includes the L1108–N1111 β-hairpin. We mutated the β-hairpin turn from VNN to SAS (a conservative change that maintains two small polar residues). $TcdA_{SAS}$ showed no defect in its cell surface binding (Fig. 3c and Supplementary Fig. 5) or *in vitro* glucosyltransfer activity (Fig. 3d and Supplementary Fig. 5) but was impaired in its capacity to kill cells (Fig. 3e). $TcdA_{SAS}$ is impaired in a cell-surface Rb^+ release assay (Fig. 3f) and in its capacity to glucosylate Rac1 in a cell-based intoxication assay (Fig. 3c), suggesting a defect in endosomal membrane insertion. The

identification of a conserved surface turn with essential function in toxicity suggests that antibodies specific for this conserved region could provide protection against multiple toxin-mediated clostridial infections and points to a generalizable strategy for generating safe vaccine antigens for this class of toxins.

Methods

Plasmid construction and point mutants

Previously described plasmids for the recombinant expression of TcdA (ref. [25]), $TcdA_{1832}$ (ref. [25]) and TcdB (ref. [18]) were used as templates for all mutant proteins generated for this study. Mutations were introduced by site-directed mutagenesis using the QuickChange protocol (Supplementary Table 4). TcdB C698A and TcdB H653A have been described previously[38]. The plasmid encoding $TcdA_{DXD}$ (ref. [27]) was provided by Ralf Gerhard (Hannover Medical School).

Protein expression and purification

GST-Rac1 was expressed and purified as described previously[25]. Toxin expression plasmids were transformed into *B. megaterium* protoplasts according to the manufacturer's protocol (MoBiTec). Transformants were grown in Luria-Bertani (LB) broth containing 10 μg ml^{-1} tetracycline at 37 °C and 220 r.p.m. overnight to produce a seed culture. To 1 l of LB, 30 ml of the overnight seed was used as inoculum. The inoculated cultures were grown at 37 °C until an optical density of 0.3–0.4 at 600 nm was reached. Protein expression was induced using 5 g l^{-1} of D-xylose solid (TCI, X0019). After a further ~4 h more at 37 °C and 220 r.p.m., the cells were harvested into 1 l bottles at 4 °C and 5,000*g* for 30 min. Pellets were resuspended in buffer containing 20 mM Tris, pH 8.0, 300 mM NaCl, 10 μg ml^{-1} DNaseI, protease cocktail (Sigma, P8849) and 20 μg ml^{-1} lysozyme. The suspensions were homogenized using a dounce homogenizer and then lysed at room temperature at 25,000 psi (Constant Cell Disruption Systems). The lysates were placed on ice then centrifuged at 18,000 r.p.m. in a JA-20 fixed-angle rotor for 25 min at 4 °C. After filtering the chilled supernatants through 0.22 mm filters, the proteins were purified using nickel affinity chromatography at 4 °C. Further purification was performed at room temperature using anion exchange chromatography followed by gel-filtration chromatography into either 20 mM Tris, pH 8.0, 100 mM NaCl (for crystallization) or 20 mM HEPES pH 6.9, 50 mM NaCl for cell-based experiments.

Crystallization

$TcdA_{1832}$ and S1329C $TcdA_{1832}$ were concentrated to 10 mg ml^{-1} in 20 mM Tris, pH 8.0, 100 mM NaCl. Crystallization was performed using the hanging drop method at 21 °C with a 1:1 ratio of protein to mother liquor. The mother liquor formulation for wild-type (WT) crystals was 100 mM Bis-Tris, pH 6, 11% PEG 4000, 30–50 mM guanidium chloride (GuCl). The mother liquor formulation for the S1329C crystals was 100 mM Bis-Tris, pH 5.8, 8% PEG 4000, 50 mM GuCl. Crystals were exchanged into appropriate mother liquor containing 20% glycerol, mounted on cryo loops and flash-cooled in liquid nitrogen.

Heavy atom derivatives of $TcdA_{1832}$ were prepared by soaking crystals in the appropriate mother liquor containing either 5 mM mercuric chloride for 90 min, 5 mM mercuric chloride for 3 days, 1 mM gold (III) chloride hydrate for 40 min, or 1 mM K_2PtCl_2 for 40 min. Heavy atom derivatives of S1329C $TcdA_{1832}$ were prepared by soaking crystals in 5 mM mercuric chloride for 3 days.

Structure determination and refinement

X-ray data were collected from single crystals on LS-CAT beamline 21 ID-D at the Advanced Photon Source (Argonne, IL) at 100 K. Diffraction data were indexed, integrated and scaled using X-ray Detector Software (XDS)[39] or HKL2000 (ref. [40]; Supplementary Table 1). The two mercury data sets were compared to the native data set using multiple isomorphous replacement with anomalous scattering in SHARP (ref. [41]). The analysis revealed five mercury sites in the two mercury data sets, differing only in their occupancies, and was consistent with the expectation that each protein monomer would have five free cysteine residues. The heavy atom positions were used to calculate initial phases, which were included in an auto-building protocol in PHENIX (ref. [42]). The fragments generated by auto-building guided manual placement of the apo-GTD structure (PDB ID 3SS1)[25]. Phases from the GTD model were combined with the phases from SHARP to calculate a new map and initiate a new round of autobuilding. The fragments generated through autobuilding allowed for manual placement of the APD (PDB ID 3H06)[28]. Phases from the combined GTD and APD model were combined with the phases from SHARP to calculate a new map and initiate new rounds of automated and manual building. Further phase improvement came from multi-crystal averaging. The working model (consisting of the GTD, most of the APD and a series of unconnected fragments from the delivery domain) was used as search model for molecular replacement into the native, platinum and gold data sets. The models and phases from each data set were subjected to multi-crystal averaging and density modification in PHENIX and resulted in excellent quality maps. One area of ambiguity was resolved through site-specific introduction of a mercury atom: crystals of a S1329C TcdA1-1832 mutant were derivatized with mercuric chloride, and the sixth heavy atom site was identified using PHENIX. The model was generated through an iterative process of manual building in Coot (ref. [43]) and refinement using Phenix[42]. The final model reflects the 50–3.25 Å native data set (*R*-factor = 18.2%, free *R*-factor = 23.7%) with 92.3% of the residues in the most favoured regions of the Ramachandran plot with 0.6% outliers. The model contains residues 4–944 and 951–1802 along with one zinc atom.

X-ray absorption spectroscopy

XAS experiments were carried out at beamline X3B of the National Synchrotron Light Source, which was equipped with a sagitally focused Si(111) double-crystal monochromator and a nickel-coated mirror for harmonic rejection. A helium Displex cryostat was used for temperature control (~15 K typical sample temperatures). Fluorescence detection was provided by a 31-element solid-state germanium detector array (Canberra). Samples of TcdA (10 mg ml^{-1}) and buffer blanks were loaded into 30 μl polycarbonate cuvettes wrapped in 1 mil Kapton tape and then frozen by immediate immersion in liquid nitrogen. The Kα fluorescence emission spectra from TcdA and buffer samples in the X-ray beam (incident energy = 10 keV) were examined. There was a significant increase in the total zinc

fluorescence counts for the TcdA sample compared with buffer, while fluorescence for the Mn–Cu series was unchanged. XAS measurements were therefore carried out at the zinc K-edge on TcdA, over an energy range of 9.46–10.3 keV. Internal energy calibration was provided by simultaneous measurement of a zinc metal foil, with the first inflection point of the edge set to a reference energy of 9,659 eV. Calibration and averaging of XAS data were carried out using Athena[44].

ICP-MS

Proteins were prepared as described above and dialysed overnight into metal-free buffers: 20 mM HEPES pH 6.9, 50 mM NaCl or 100 mM Bis-Tris pH 6.0, 50 mM NaCl at 4 °C. Samples analysed in the presence of InsP6 were dialysed in buffer containing 10 mM InsP6. Samples analysed in the presence of TPEN were dialysed in 1 mM TPEN for 8 h at room temperature. Buffers containing 10 μM $ZnCl_2$ and 1 mM TCEP were used to add zinc back to the protein. Protein samples were analysed for metal content by using 50 μl of the protein solution and diluting in 2.5% (vol/vol) nitric acid (Sigma-Aldrich, TraceSELECT quality) to a final volume of 3 ml for ICP-MS analysis. In samples with significant precipitation after acidification, the samples were centrifuged at 15,000*g* for 20 min to pellet any precipitate, and the solution was transferred to a fresh tube for measurement. The diluted samples were analysed for ^{66}Zn, ^{55}Mn, ^{63}Cu and ^{60}Ni using a 1–30 ppb standard curve using stock solutions (Perkin Elmer). Analyses were performed using a PerkinElmer ELAN DRCII ICP-MS. The instrument was equipped with a Microflow PFA-ST concentric nebulizer with a 100 μl min^{-1} self-aspiration capillary, a cyclonic spray chamber, a quartz torch and nickel sampler/skimmer cones. Germanium at 50 ppb was added as an internal standard using an EzyFit glass mixing chamber. Concentrations (in ppb) were corrected for the dilution factor, and the molar concentrations and molar ratios (^{66}Zn/protein) were determined for each sample.

Autoprocessing assays

Assays were performed as described previously[38]. Reactions testing the effect of TPEN were pre-incubated with 10 mM TPEN at 37 °C for 2 h before the addition of InsP6. Autoprocessing assays with samples also analysed by ICP-MS were performed in the appropriate dialysate and indicated reactions contained 100 nM InsP6 pre-treated with TPEN to remove zinc from the InsP6 stock solution. Gels were quantified using ImageJ[45]. The intensity associated with cleaved GTD was divided by the intensity for the intact protein in the absence of InsP6.

Cell lines

Chinese hamster ovary (CHO-K1), HeLa and Vero cells were authenticated and verified to be mycoplasma-free at the time of purchase from ATCC and were aliquoted into primary frozen stocks. Experiments were conducted in cells passaged less than 30 times from the frozen stock.

Viability assays

CHO-K1 cells were cultured in Ham's F-12 medium with 10% FBS and 1% penicillin and streptomycin and seeded at a concentration of 8,000 cells per well in 96-well CellBind plates. The next day, medium was exchanged with serum-free medium and cells were intoxicated by adding TcdA toxins at a serial dilution of 1/3 starting at 10 nM. After intoxication, cells were incubated at 37 °C, 5% CO_2 for 48 h. FBS was added back to cells 24 h after intoxication to a final concentration of 10% (vol/vol). The cell viability after 48 h was assessed by PrestoBlue Cell Viability Reagent (Life Technologies). Fluorescence was read on a Spectramax M5 plate reader (Molecular Devices).

Rubidium release assays

$^{86}Rb^{+}$ release assay was performed as previously reported[2] with slight modifications. Briefly, Vero cells were seeded in 24-well plates in the medium (DMEM with 10% FBS), supplemented with 1 μCi ml^{-1} $^{86}Rb^{+}$ (PerkinElmer) at a density of 1×10^5 cells per well. Cells were incubated at 37 °C, 5% CO_2 overnight. Medium was exchanged with fresh growth medium with 100 nM bafilomycin A1 (Sigma) and continued to incubate for another 20 min. Cells were then chilled on ice and ice-cold medium containing TcdA mutants (10 nM) was added. Cells were kept on ice for toxin binding for 1 h at 4 °C before they were washed with ice-cold PBS twice to remove unbound toxins. pH-dependent insertion into the plasma membrane was induced by warm, acidified growth medium (37 °C, pH 4.8 or pH 7.5) for 5 min at 37 °C. Cells were incubated further on ice, medium containing released $^{86}Rb^{+}$ was removed from the cell plate at different time points, and the amount of $^{86}Rb^{+}$ released was determined by liquid scintillation counting with TopCount NXT (PerkinElmer). The percentage of $^{86}Rb^{+}$ release was calculated by subtracting the signal from untreated controls from each time point and dividing this difference by the signal from cells treated with 0.1% Triton.

Cell binding and Rac1 glucosylation in cells

HeLa cells were synchronized by cooling to 4 °C and then intoxicated with 10 nM toxin or buffer. The cells were returned to 4 °C for 1 h and then shifted to 37 °C for 3 h. The cells were harvested and lysed (250 mM sucrose, 10 mM Tris pH 7.5, 3 mM imidazole), samples were boiled, and proteins were separated by SDS–polyacrylamide gel electrophoresis (PAGE). Samples were analysed by western blot with primary antibodies specific for TcdA CROPS (Abcam, ab19953), unglucosylated Rac1 (BD, 610650) and total Rac1 (Millipore, clone 23A8). Binding of an anti-mouse, HRP-conjugated secondary antibody (Jackson ImmunoResearch Laboratories, 115-035-174) was detected with a LumiGLO kit (Cell Signaling) according to the manufacturer's instructions.

Rac1 glucosylation *in vitro*

Toxin (100 nM) was added to 0.8 μM GST-Rac1 and 25 μM UDP-glucose (Sigma) in glucosylation buffer (50 mM HEPES pH 6.9, 100 mM KCl, 2 mM $MgCl_2$, 1 mM $MnCl_2$) for 3 h. The reactions were stopped by adding Laemmli buffer and boiling. Samples were separated by SDS-PAGE and analysed by western blot using antibodies specific for glucosylated and total Rac1.

Statistical analyses

No statistical method was used to predetermine the sample size. Error bars displayed throughout the manuscript represent standard deviation (s.d.) and were calculated from biological replicates. No data were excluded from analysis. The number of replicates for each experiment is indicated in the figure legends.

Supplementary Material

Refer to Web version on PubMed Central for supplementary material.

Acknowledgments

This research was supported by NIAID of the National Institutes of Health (award no. R01AI095755 to D.B.L.) and NIGMS (award no. R01GM042569 to D.P.G.). The authors thank staff at the LS-CAT beamline for help with data collection. Use of the Advanced Photon Source, an Office of Science User Facility operated for the US Department of Energy (DOE) Office of Science by Argonne National Laboratory, was supported by the US DOE under contract no. DE-AC02-06CH11357. Use of LS-CAT Sector 21 was supported by the Michigan Economic Development Corporation and the Michigan Technology Tri-Corridor (grant no. 085P1000817). Use of the National Synchrotron Light Source, Brookhaven National Laboratory, was supported by the US DOE, Office of Science, Office of Basic Energy Sciences (contract no. DE-AC02-98CH10886). Operations at the NSLS beamline X3B were supported by NIH P30-EB009998.

References

1. Lyerly DM, Krivan HC, Wilkins TD. *Clostridium difficile*: its disease and toxins. Clin Microbiol Rev. 1988; 1:1–18. [PubMed: 3144429]
2. Kelly CP, LaMont JT. *Clostridium difficile*—more difficult than ever. N Engl J Med. 2008; 359:1932–1940. [PubMed: 18971494]
3. Voth DE, Ballard JD. *Clostridium difficile* toxins: mechanism of action and role in disease. Clin Microbiol Rev. 2005; 18:247–263. [PubMed: 15831824]
4. Jank T, Aktories K. Structure and mode of action of clostridial glucosylating toxins: the ABCD model. Trends Microbiol. 2008; 16:222–229. [PubMed: 18394902]
5. Lessa FC, et al. Burden of *Clostridium difficile* infection in the United States. N Engl J Med. 2015; 372:825–834. [PubMed: 25714160]
6. Lowy I, et al. Treatment with monoclonal antibodies against *Clostridium difficile* toxins. N Engl J Med. 2010; 362:197–205. [PubMed: 20089970]
7. Frey SM, Wilkins TD. Localization of two epitopes recognized by monoclonal antibody PCG-4 on *Clostridium difficile* toxin A. Infect Immun. 1992; 60:2488–2492. [PubMed: 1375199]
8. Orth P, et al. Mechanism of action and epitopes of *Clostridium difficile* toxin B-neutralizing antibody bezlotoxumab revealed by X-ray crystallography. J Biol Chem. 2014; 289:18008–18021. [PubMed: 24821719]
9. Sauerborn M, Leukel P, von Eichel-Streiber C. The C-terminal ligand-binding domain of *Clostridium difficile* toxin A (TcdA) abrogates TcdA-specific binding to cells and prevents mouse lethality. FEMS Microbiol Lett. 1997; 155:45–54. [PubMed: 9345763]
10. Frisch C, Gerhard R, Aktories K, Hofmann F, Just I. The complete receptor-binding domain of *Clostridium difficile* toxin A is required for endocytosis. Biochem Biophys Res Commun. 2003; 300:706–711. [PubMed: 12507507]
11. Florin I, Thelestam M. Lysosomal involvement in cellular intoxication with *Clostridium difficile* toxin B. Microb Pathog. 1986; 1:373–385. [PubMed: 3508493]
12. Qa'Dan M, Spyres LM, Ballard JD. pH-induced conformational changes in *Clostridium difficile* toxin B. Infect Immun. 2000; 68:2470–2474. [PubMed: 10768933]
13. Barth H, et al. Low pH-induced formation of ion channels by *Clostridium difficile* toxin B in target cells. J Biol Chem. 2001; 276:10670–10676. [PubMed: 11152463]

14. Just I, et al. The enterotoxin from *Clostridium difficile* (ToxA) monoglucosylates the Rho proteins. J Biol Chem. 1995; 270:13932–13936. [PubMed: 7775453]
15. Just I, et al. Glucosylation of Rho proteins by *Clostridium difficile* toxin B. Nature. 1995; 375:500–503. [PubMed: 7777059]
16. Egerer M, Giesemann T, Jank T, Satchell KJ, Aktories K. Auto-catalytic cleavage of *Clostridium difficile* toxins A and B depends on cysteine protease activity. J Biol Chem. 2007; 282:25314–25321. [PubMed: 17591770]
17. Reineke J, et al. Autocatalytic cleavage of *Clostridium difficile* toxin B. Nature. 2007; 446:415–419. [PubMed: 17334356]
18. Pruitt RN, Chambers MG, Ng KK, Ohi MD, Lacy DB. Structural organization of the functional domains of *Clostridium difficile* toxins A and B. Proc Natl Acad Sci USA. 2010; 107:13467–13472. [PubMed: 20624955]
19. Albesa-Jove D, et al. Four distinct structural domains in *Clostridium difficile* toxin B visualized using SAXS. J Mol Biol. 2010; 396:1260–1270. [PubMed: 20070948]
20. Ho JG, Greco A, Rupnik M, Ng KK. Crystal structure of receptor-binding C-terminal repeats from *Clostridium difficile* toxin A. Proc Natl Acad Sci USA. 2005; 102:18373–18378. [PubMed: 16344467]
21. Murase T, et al. Structural basis for antibody recognition in the receptor-binding domains of toxins A and B from *Clostridium difficile*. J Biol Chem. 2014; 289:2331–2343. [PubMed: 24311789]
22. Olling A, et al. The combined repetitive oligopeptides of *Clostridium difficile* toxin A counteract premature cleavage of the glucosyl-transferase domain by stabilizing protein conformation. Toxins (Basel). 2014; 6:2162–2176. [PubMed: 25054784]
23. Zhang Y, Hamza T, Gao S, Feng H. Masking autoprocessing of *Clostridium difficile* toxin A by the C-terminus combined repetitive oligo peptides. Biochem Biophys Res Commun. 2015; 459:259–263. [PubMed: 25725153]
24. Jank T, Giesemann T, Aktories K. *Clostridium difficile* glucosyltransferase toxin B-essential amino acids for substrate binding. J Biol Chem. 2007; 282:35222–35231. [PubMed: 17901056]
25. Pruitt RN, et al. Structural determinants of *Clostridium difficile* toxin A glucosyltransferase activity. J Biol Chem. 2012; 287:8013–8020. [PubMed: 22267739]
26. Rupnik M, et al. Characterization of the cleavage site and function of resulting cleavage fragments after limited proteolysis of *Clostridium difficile* toxin B (TcdB) by host cells. Microbiology. 2005; 151:199–208. [PubMed: 15632438]
27. Kreimeyer I, et al. Autoproteolytic cleavage mediates cytotoxicity of *Clostridium difficile* toxin A. Naunyn Schmiedebergs Arch Pharmacol. 2011; 383:253–262. [PubMed: 21046073]
28. Pruitt RN, et al. Structure–function analysis of inositol hexakisphosphate-induced autoprocessing in *Clostridium difficile* toxin A. J Biol Chem. 2009; 284:21934–21940. [PubMed: 19553670]
29. Puri AW, et al. Rational design of inhibitors and activity-based probes targeting *Clostridium difficile* virulence factor TcdB. Chem Biol. 2010; 17:1201–1211. [PubMed: 21095570]
30. Shen A, et al. Defining an allosteric circuit in the cysteine protease domain of *Clostridium difficile* toxins. Nature Struct Mol Biol. 2011; 18:364–371. [PubMed: 21317893]
31. von Eichel-Streiber C, Laufenberg-Feldmann R, Sartingen S, Schulze J, Sauerborn M. Comparative sequence analysis of the *Clostridium difficile* toxins A and B. Mol Gen Genet. 1992; 233:260–268. [PubMed: 1603068]
32. Zhang Z, et al. Translocation domain mutations affecting cellular toxicity identify the *Clostridium difficile* toxin B pore. Proc Natl Acad Sci USA. 2014; 111:3721–3726. [PubMed: 24567384]
33. Genisyuerek S, et al. Structural determinants for membrane insertion, pore formation and translocation of *Clostridium difficile* toxin B. Mol Microbiol. 2011; 79:1643–1654. [PubMed: 21231971]
34. Choe S, et al. The crystal structure of diphtheria toxin. Nature. 1992; 357:216–222. [PubMed: 1589020]
35. Wang J, London E. The membrane topography of the diphtheria toxin T domain linked to the a chain reveals a transient transmembrane hairpin and potential translocation mechanisms. Biochemistry. 2009; 48:10446–10456. [PubMed: 19780588]

36. Pettersen EF, et al. UCSF Chimera—a visualization system for exploratory research and analysis. J Comput Chem. 2004; 25:1605–1612. [PubMed: 15264254]

37. Teichert M, Tatge H, Schoentaube J, Just I, Gerhard R. Application of mutated *Clostridium difficile* toxin A for determination of glucosyltransferase-dependent effects. Infect Immun. 2006; 74:6006–6010. [PubMed: 16988280]

38. Chumbler NM, et al. *Clostridium difficile* toxin B causes epithelial cell necrosis through an autoprocessing-independent mechanism. PLoS Pathogens. 2012; 8:e1003072. [PubMed: 23236283]

39. Kabsch W. XDS. Acta Crystallogr D. 2010; 66:125–132. [PubMed: 20124692]

40. Otwinowski, Z.; Minor, W. Methods in Enzymology Vol. 276: Macromolecular Crystallography, part A. Carter, CW., Jr; Sweets, RM., editors. Academic; 1997. p. 307-326.

41. Bricogne G, Vonrhein C, Flensburg C, Schiltz M, Paciorek W. Generation, representation and flow of phase information in structure determination: recent developments in and around SHARP 2.0. Acta Crystallogr D. 2003; 59:2023–2030. [PubMed: 14573958]

42. Adams PD, et al. PHENIX: building new software for automated crystallographic structure determination. Acta Crystallogr D. 2002; 58:1948–1954. [PubMed: 12393927]

43. Emsley P, Cowtan K. Coot: model-building tools for molecular graphics. Acta Crystallogr D. 2004; 60:2126–2132. [PubMed: 15572765]

44. Ravel B, Newville M. ATHENA, ARTEMIS, HEPHAESTUS: data analysis for X-ray absorption spectroscopy using IFEFFIT. J Synchrotron Radiat. 2005; 12:537–541. [PubMed: 15968136]

45. Schneider CA, Rasband WS, Eliceiri KW. NIH image to ImageJ: 25 years of image analysis. Nature Methods. 2012; 9:671–675. [PubMed: 22930834]

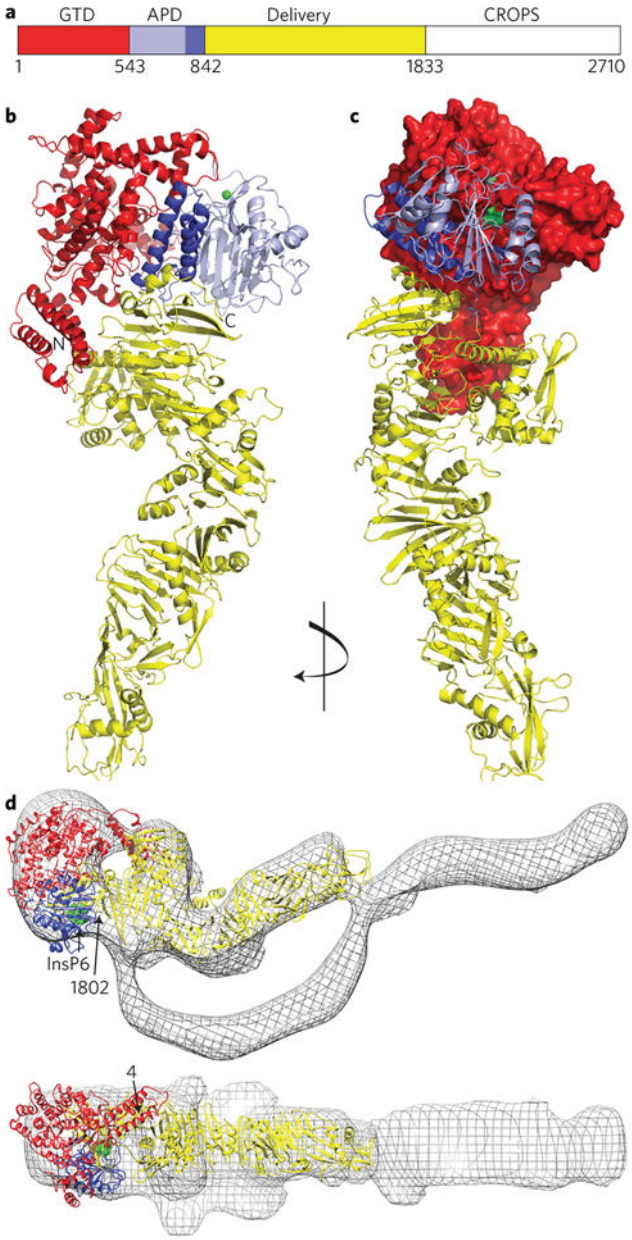

Figure 1. Structure of TcdA

a, The TcdA primary structure can be divided into four functional domains: the glucosyltransferase domain (GTD, red), the autoprotease domain (APD, purple; including the three-helix bundle, dark purple), the delivery domain (yellow) and the CROPS domain (white). **b**, Cartoon representation of the $TcdA_{1832}$ structure (coloured according to **a**), with zinc shown in green. **c**, The structure in **b**, rotated 90°, with the GTD shown as a surface view with the UDP–glucose binding site in green. **d**, The $TcdA_{1832}$ structure was fit in the 20 Å EM map of TcdA holotoxin[18] using Chimera[36]. The InsP6 binding site is shown in green, and positions for the first and last residues visible in the structure are indicated.

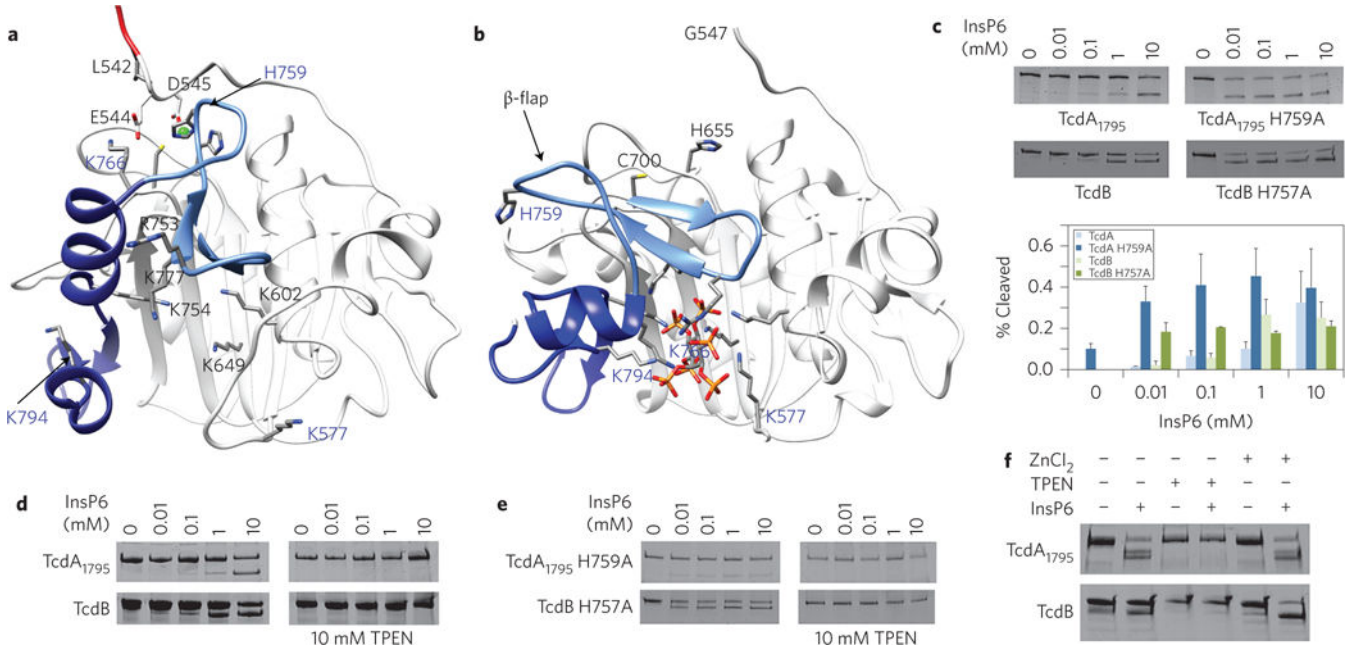

Figure 2. Zinc is required for autoprocessing activity

a, The APD, along with a small portion of the GTD and the three-helix bundle from the $TcdA_{1832}$ structure (oriented as in Fig. 1a), is depicted with residue 542 in red, residues 543–745 in white, the 746–765 β-flap in light blue, and some of the three-helix bundle (766–801) in dark blue. Zinc (green) is bound in the APD active site by H655, C700 and H759. Four lysines form the initial binding site for InsP6: K602, K649, K754 and K777. **b**, On comparison with **a**, the InsP6-bound structure of the TcdA APD (Protein Data Bank: 3HO6)[28] suggests significant structural changes occur with InsP6 binding: the accumulation of eight lysines and one arginine in the InsP6-binding site, a rearrangement of the β-flap and elements of the three-helix bundle, and displacement of H759 from the active site. **c**, Mutation of TcdA His759 or TcdB His757 leads to proteins that undergo autoprocessing at lower concentrations of InsP6. Cleaved GTD was quantified relative to the holotoxin in the 0 mM InsP6 control, and means ± s.d. (n = 3) are shown. **d**, Chelation of zinc through treatment with 10 mM TPEN renders TcdA and TcdB incapable of InsP6-induced autoprocessing. **e**, Chelation of zinc in mutants that show enhanced autoprocessing renders TcdA and TcdB incapable of InsP6-induced autoprocessing. Experiments in **d**,**e** were conducted in the presence of 5% ethanol, a solvent for TPEN. **f**, Autoprocessing can be restored in TPEN-treated autoprocessing-defective preparations of TcdA and TcdB with the addition of $ZnCl_2$. Gels in **c–f** are representative of three independent experiments.

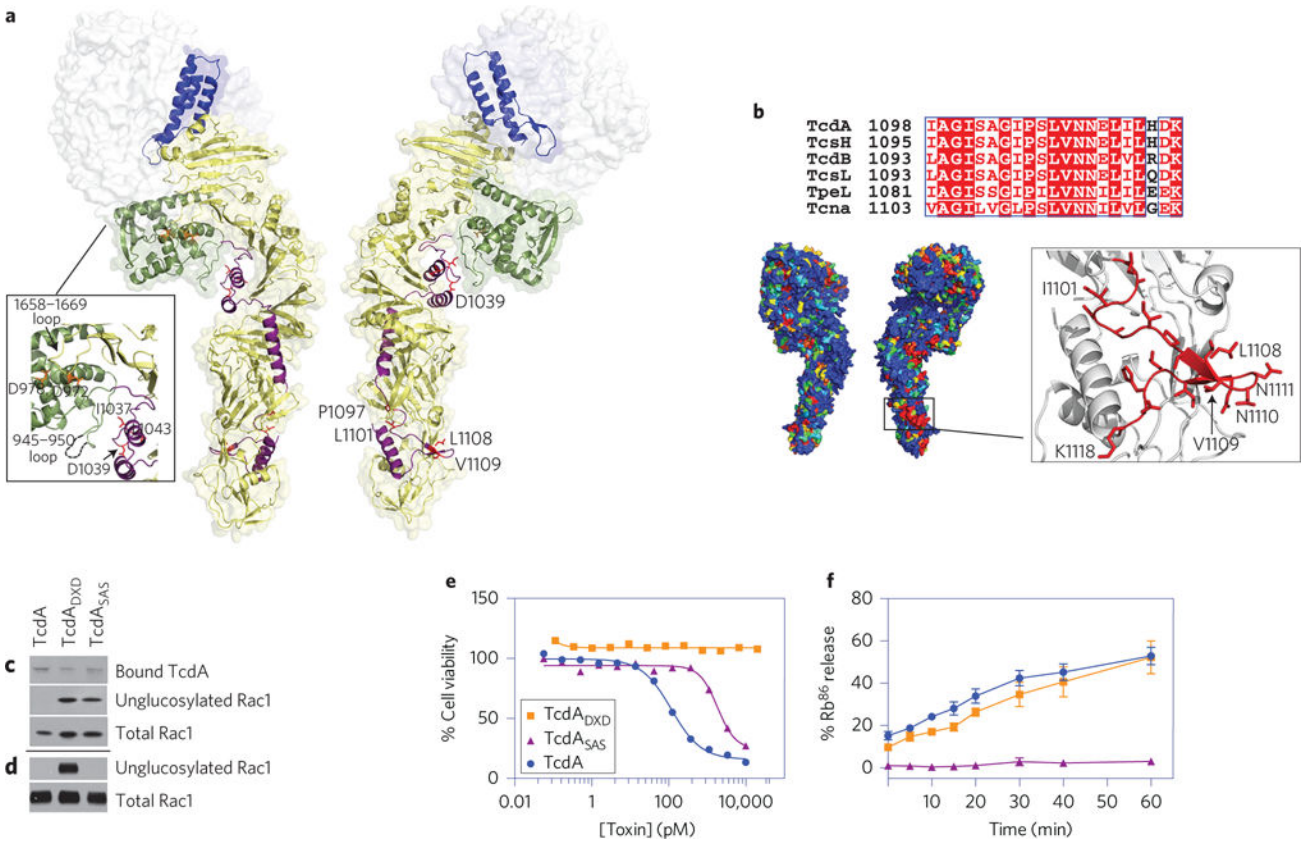

Figure 3. The delivery domain provides an extended scaffold for an α-helical hydrophobic stretch involved in pore formation

a, Most of the $TcdA_{1832}$ crystal structure (residues 1–1025 and 1136–1802) is depicted as a transparent surface with the GTD in white and the APD in blue. The delivery domain is visible as a cartoon to highlight the three-helix bundle (blue), the globular sub-domain (green), the α-helical hydrophobic stretch (residues 1026–1135, pink) and the β-scaffold (yellow). Residues implicated in TcdB pore formation are shown as orange[33] or red[32] sticks. **b**, Representative sequences from the six large clostridial glycosylating toxins were aligned and scored with a Risler matrix according to the extent of sequence variation. Scores are displayed on the $TcdA_{1832}$ structure surface with a colour ramp (red, orange, yellow, green, light blue, dark blue) in which strictly conserved residues are coloured red and the most variable residues are coloured dark blue. The most conserved surface region (boxed) is at the end of the α-helical hydrophobic stretch: the 1098–1118 loop and β-hairpin. Within this region, the V1109, N1110 and N1111 residues are notable in their accessibility to solvent. **c**, The $TcdA_{SAS}$ protein binds cells at levels equivalent to wild type but is impaired in its capacity to glucosylate Rac1. Toxins (10 nM) were applied to HeLa cells and incubated for 3 h at 37 °C. Proteins were separated by SDS-PAGE and probed with antibodies that recognize TcdA CROPS, non-glucosylated Rac1 or total Rac1. Quantitation of four gels indicates that while 100% of the detectable Rac1 was glucosylated by TcdA, only 23.4 ± 10.8% was glucosylated by $TcdA_{SAS}$ (relative to mock treated). **d**, The $TcdA_{SAS}$ protein is not impaired in its capacity to glucosylate Rac1 *in vitro* using purified proteins. Toxins (100 nM) were incubated with purified GST-Rac1 for 3 h at 37 °C and analysed as in c. The gel is

representative of three independent experiments. **e**, The $TcdA_{SAS}$ mutant is defective in its cellular toxicity. Toxins (10 fM–20 nM) were incubated with CHO cells for 48 h at 37 °C and viability was normalized to untreated cells. A representative dose–response curve is shown and values of the effective concentration conferring half maximal protection (EC_{50}) ± s.d. were calculated from two biological replicates using Prism: TcdA (blue circles, EC_{50} = 0.11 ± 0.01 nM); $TcdA_{DXD}$ (a glucosyltransferase-defective mutant[37]; orange squares, EC_{50} > 20 nM); $TcdA_{SAS}$, (purple triangles, EC_{50} = 1.74 ± 0.39 nM). **f**, Pore formation on biological membranes. TcdA, $TcdA_{DXD}$ and $TcdA_{SAS}$ were applied to Vero cells preloaded with $^{86}Rb^{+}$ and then subjected to external medium at pH 4.8. Data represent the means and s.d. associated with four experiments. Colours are as in **e**.